# Failure and Stabilization Mechanisms in Multiply Cycled Conducting Polymers for Energy Storage Devices

**ARTICLE** *in* THE JOURNAL OF PHYSICAL CHEMISTRY C · SEPTEMBER 2010

Impact Factor: 4.77 · DOI: 10.1021/jp105965u



**5 AUTHORS**, INCLUDING:

Levi Mikhael
Bar Ilan University
**193** PUBLICATIONS **8,725** CITATIONS
SEE PROFILE

Doron Aurbach
Bar Ilan University
**535** PUBLICATIONS **21,810** CITATIONS
SEE PROFILE

Renaud Demadrille
Atomic Energy and Alternative Energies Co…
**63** PUBLICATIONS **1,168** CITATIONS
SEE PROFILE

Adam Pron
Warsaw University of Technology
**345** PUBLICATIONS **8,099** CITATIONS
SEE PROFILE

# Failure and Stabilization Mechanisms in Multiply Cycled Conducting Polymers for Energy Storage Devices

**Naomi Levy,[†] Mikhael D. Levi,*[,†] Doron Aurbach,[†] Renaud Demadrille,[‡] and Adam Pron[‡]**

*Department of Chemistry, Bar-Ilan University, Ramat-Gan 52900, Israel, and INAC/SPrAM (UMR 5819 CEA-CNRS-Univ. J. Fourier-Grenoble I), Laboratoire d'Electronique Moléculaire Organique et Hybride, CEA, Grenoble, 17 rue des Martyrs, 38054 Grenoble, France*

*Received: June 28, 2010*

We report herein new results on the application of the electrochemical quartz crystal microbalance (EQCM) method to study multiple cycling electrodes comprising improved poly-3-octylthiophene (P3OTh) films under various conditions. Emphasis is given to the n-doped P3OTh films with their retarded initial kinetics of doping due to the negative charge carriers and solvent trapping. Further tests included studying the release of trapped charges and solvent during p-redoping and assessing the interactions between the oppositely charged carriers via a coupled (intermittent) n-p-doping in the widest potential window of 3.3 V. A complete deconvolution of the EQCM response in terms of the contributing counterion, co-ion, and solvent fluxes has been done. A remarkable feature discovered was a gradual decrease of exchangeable solvent molecules in the films as a result of their long-term cycling and cycling conditions. This was correlated to a gradual progressing of the n-type carriers trapping at high and long-term cathodic polarization of the films (confirmed by impedance and UV−vis spectropies and by in situ conductance measurements). The unique information obtained about long-term cycling of P3OTh films under various conditions is used to create a broader context of evaluation of cycling ability of conducting polymer electrodes, compared to typical Li-insertion electrodes. The present studies render applications of EQCM for more complicated systems such as nanocomposites comprising conducting polymer and carbon nanotubes that can be used as superb electrode's materials for advanced supercapacitors.

## Introduction

Electronically conducting polymers (ECP), a vast and highly important class of new organic materials, was in the focus of pioneering and intensive research work during last 20−25 years;[1−5] as a result of these concentrated efforts, they find nowadays various practical applications.[6,7] Unusual properties of these conducting plastic materials originate from the macromolecules possessing $\pi$-conjugation in the backbones, allowing their facile chemical (or electrochemical) reversible oxidation/reduction. This typical redox process (also called doping) consists of injection of electronic charge carriers onto macromolecular chains, which are electrostatically screened by the counterions (e.g., by $I_3^-$ when $I_2$ vapor is used as an oxidant in the process called chemical doping)[8] or by the ions transported from the bath solution (i.e., the electrochemical doping induced by the electrode polarization).[9] The variation of the electrode potential by some 600−700 mV (depending on the polymer structure) brings about an insulator-to-metal phase transition in the polymer bulk accompanied by increase in the electronic conductivity by 8−10 orders of magnitude.[8] In their undoped state, $\pi$-conjugated oligomers and polymers are typical organic semiconductors. When moderately doped they behave as organic conductors, and when heavily doped they show metallic-type conductivity in some cases.[10] The major commercialization of the ECPs for fabrication of organic light-emitting diodes (OLEDs)[11] is based on their ability to perfectly match the requirements of a readily processable,[12] high-quality organic semiconductor. Other possible applications may include solid-state memory devices,[13] photovoltaic cells,[14] organic thin-film transistors (OTFT),[15] and other devices.[16] Recently two special issues of *Advanced Materials* devoted to ECP-based organic electronics have been published.[17]

Applications of the ECPs in their heavily doped state with typically high electronic conductivity have not yet been commercialized. This is due to a number of reasons, which initially were associated with difficult control of the polymer chain structure and its macromolecular parameters such as the molecular mass and its large distribution. These problems were partially bypassed via a significant progress in the synthesis of regioregular conjugated polymers leading to macromolecular compounds of controlled chain microstructure and reduced poly dispersity.[18,19] However, a really complicated charge compensation mechanism during electrochemical doping of these polymers still remains a problem.[20,21] This includes coupled ionic and solvent fluxes into/from the polymer-based electrodes, resulting in their considerable dimensional changes.[22,23] It was early recognized that the ECPs can be used as an anion-exchange cathode in a couple with Li metal anode in aprotic Li salt solutions for rechargeable polyaniline-lithium battery (Bridgestone Corpor., Japan).[24] However, their commencing commercialization as such in early 90s was soon discontinued in view of the overwhelming advantage of the competing rechargeable cathodes based on lithiated transition metal oxides, such as $Li_xCoO_2$. The latter electrode was suitable for utilization in a conceptually new rechargeable Li ion battery for which Li-ion conducting cathode was required. Although the typical p-doped conducting polymers such as polyaniline, poly-

* To whom correspondence should be addressed. E-mail: levimi@mail.biu.ac.il.
† Bar-Ilan University.
‡ Laboratoire d'Electronique Moléculaire Organique et Hybride.

10.1021/jp105965u 
Published on Web 09/10/2010

thiophene, polypyrrole, poly-*p*-phenylene, etc. can be switched from the anion- to cation-exchange properties, using the concept of auto (or self) doping[25] or forming an intimate blend with a polymeric ionomer (containing fixed anionic functionalities),[26] the ECPs still fail in terms of the specific capacity attained, long-term cyclability, constancy of the charge and discharge voltage,[27] when comparing these characteristics with that for $Li_xCoO_2$ or very popular nowadays $Li_xMPO_4$ olivines.[28]

On the other hand, ECPs are considered to be attractive positive electrodes for building asymmetric activated carbon/ECP electric double layer (super)capacitors (EDLC) cells.[29] In contrast to Li-ion batteries, the anion-exchanging character of the p-doped ECP cathodes is no more a barrier to their proper functioning in these devices; in addition, the specific energy and power of asymmetric EDLC are higher than those of the symmetric EDLC based on activated carbon electrodes.[29] As in the case of Li-ion batteries (vide supra), a strong competition from the class of inorganic cathodes for EDLC, e.g., a-$MnO_2$, can be expected. Selection of the best material will be eventually made on the basis of demonstration of a higher specific energy and power and better cyclability.

The electrochemical quartz crystal microbalance method (EQCM) has been extensively used to study charge compensation mechanisms in ECPs during their electrochemical cycling, linking the total changes of the electrode's mass to the contributing counter- and co-ion fluxes and to the flux of the solvent molecules.[20−22] Although this mechanism was shown to broadly depend on the chemical and morphological structure of the polymers used, and hence, on the mode of their preparation, the related EQCM studies referred mainly to a limited number of (predominantly) p-doping cycles (fewer papers addressed the n-doping mechanism).[30] Surprisingly, except for a recent paper on the behavior of the polypyrrole/polystyrene sulfonate blend electrode cycled in a variety of aqueous electrolyte solutions,[31] EQCM has not been yet used for studies of cycling performance of ECPs. The utilization of this technique may be of exceptional importance in characterizing changes in the ionic/solvent fluxes in the polymeric electrode induced by long-term cycling, especially in combination with in situ conductivity, vis/NIR, and electrochemical impedance spectroscopy, which are able to signify about possible coupled changes in its chemical and electronic structure.

Independent of their nature, ECPs were reported to rank much below the Li-insertion inorganic hosts in their cyclability[27] but may be much more advantageous for special applications, such as in flexible organic (or all-plastic) batteries.[32] The goal of the present paper is to provide insight into failure and stabilization mechanisms during long-term cycling of conducting polymer electrodes. Simple cheap, commercially available (homo)polymers such as polypyrrole, polythiophene, polyaniline, etc. are the best model choice for such an investigation. Since we were interested in studying multiple n-doping cycling and coupled n-p-doping cycling, thin films of poly-3-octylthiophene (P3OTh), cycled in acetonitrile-based electrolyte solutions, seemed to be the most suitable system to be investigated. The electrochemical preparation of such films was optimized to ensure both sufficiently good cycling performance and suitability for the EQCM measurements (see Experimental section).

We report herein on doping induced fluxes of ions and solvent molecules assessed by the application of EQCM to the *entire* cycling life of P3OTh electrodes. By use of a variety of techniques in addition to EQCM, we identified two possibly correlated factors which limit long-term cyclability of these electrodes under various cycling conditions: deepening localization of the n-type charge carriers, and a progressive loss of the exchangeable solvent content as a function of cycle number and cycling conditions. On the basis of the established failure mechanism of the capacity retention in P3OTh cathodes and anodes, possible routes for improving the cycling life of conducting polymer electrodes are discussed.

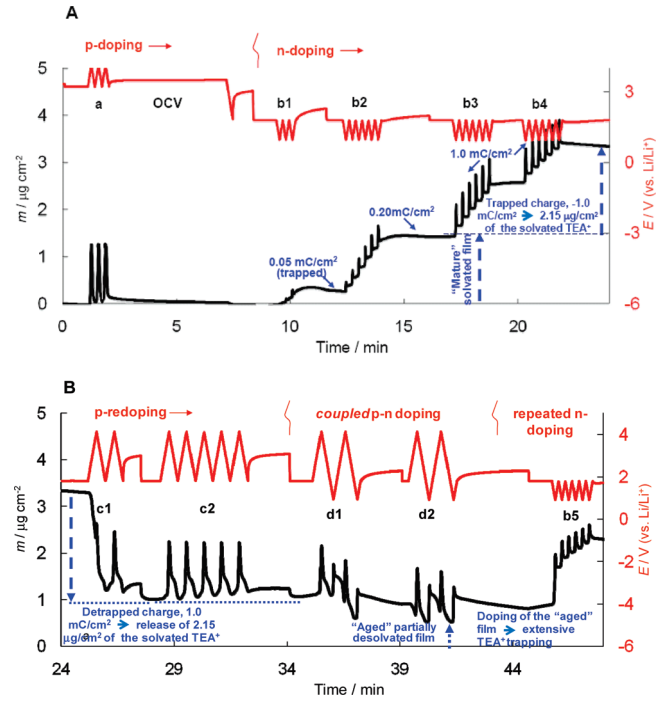


**Figure 1.** The mass and electrode potential vs time plots for a P3OTh film-coated Pt-plated quartz crystal during the course of long-term EQCM test. Potential scan rate, $\nu = 100$ mV $s^{-1}$. The cycling was performed in the following order (details are explained in the body of the text). (A) (1) Initial p-doping of the fresh film between 3.2 and 4.13 V (vs $Li/Li^+$ in PC), a1; (2) n-doping between 1.80 and 0.95 V (b1−b2) and between 1.80 and 0.92 V (b3−b4). (B) (1) p-redoping up 4.13 V and further p-doping between this potential and 1.8 V (c1−c2); (2) coupled n-p-doping between 0.92 and 4.13 V (d1−d2); (3) repeated n-doping between 1.80 and 0.92 V (b5).

## Results and Discussion

**Stages of the Multiple Cycling Test of P3OTh Film Electrodes Studied by Cyclic Voltammetry (CV) and EQCM.** Figure 1 shows raw plots of the mass and electrode potential of the P3OTh film (the black and the red lines, respectively) vs time for the entire cycling test under different cycling conditions. The type of the process is indicated in the red script in the top of the figure, and by the black Latin letters below (e.g., $a$ = p-doping, $b$ = n-doping, etc.) with the subsequent number, determining the place of the group in the entire cycling test. For example, b1−b4 reflect 4 consecutive n-doping potential scans, each consisting of 6 cycles (thus, e.g. b4−6 means the sixth cycle in the b4 (n-doping) cycling group). Afterward, c and d mean p-redoping and a coupled n-p-doping, respectively, whereas the final stage of the test is the repeated n-doping in its native potential domain, denoted as b5 in panel B (the related potential domains are indicated in the figure's caption). The CVs measured simultaneously with the EQCM response are shown in Figure 2 from stages a to c, i.e., for the initial p-doping, the subsequent n-doping, and for the p-redoping.

Table 1 summarizes the charge densities for the positive and negative potential scans, $Q_+$ and $Q_-$, the related Faradaic efficiencies (FE), and the doping levels of the P3OTh film

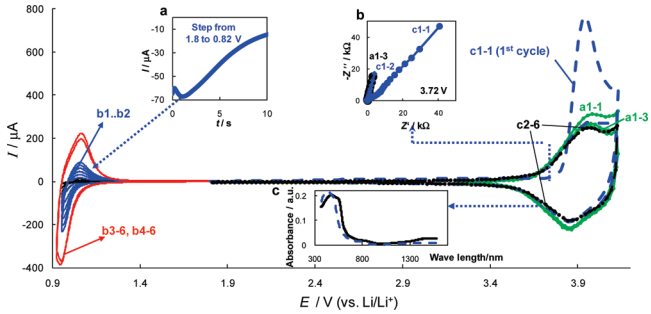


**Figure 2.** A series of CVs for the P3OTh film-coated quartz crystal measured simultaneously with the EQCM response shown in A and B of Figure 1 (the stages of the entire cycling test are denoted by the same symbols). Scan rate $\nu = 100$ mV s$^{-1}$. Insets a, b, and c relate to separate experiments with a similar P3OTh film coated onto an Pt wire used for the potential step chronoamperometry (a) and electrochemical impedance measurements (b) in the potential domains indicated (the link is shown by the dotted blue lines). Inset (c) relates to the optical absorption spectra from a similar P3OTh film coated on an ITO electrode for the fresh (the black curve) and the "aged" film, which was preliminary n-doped at the potential 0.8 V during 3 min and then subsequently p-redoped (the broken blue curve in inset c).

**TABLE 1: Charge Densities for the Positive and Negative Potential Scans, $Q_+$ and $Q_-$, the Related FEs, and the Doping Levels of the P3OTh Film Obtained from Selected CVs of the Entire Cycling Test**

| cycle no. | $Q_+$/mC cm$^{-2}$ | $-Q_-$/mC cm$^{-2}$ | FE/% | doping level |
|---|---|---|---|---|
| a1−3 | 0.66 | 0.61 | 92 | 0.240 |
| b1−3 | 0.0095 | 0.033 | 29 | 0.004 |
| b2−6 | 0.089 | 0.126 | 71 | 0.035 |
| b4−6 | 0.242 | 0.293 | 83 | 0.095 |
| c2−6 | 0.642 | 0.569 | 89 | 0.226 |
| b5−6 | 0.236 | 0.344 | 69 | 0.094 |

derived from the selected CV curves of the cycling test. It is seen that p-doping of the film is a reversible process with a fairly good (for a thin film) FE of 92% and a typical doping level of 0.24 e$^-$ per repeat unit of the macromolecule. The periodic mass changes accompanying the p-doping process are very stable as seen from Figure 1a. We intentionally limited the number of p-doping cycles (a series) to be sure that the doping-undoping induced changes in the morphology and the structure of the films will not affect to a large extent the subsequent n-doping process.

The n-doping commences at a drastically slower rate compared to that of the p-doping, as is seen from the gradual increase in the CV current during stages b1 and b2 (the blue curves in Figure 2) with the concomitant gradual increase in the film's mass (see also the related data in Table 1). These initial n-doping cycles have poor but yet improving with cycling FE (see Table 1). We ascribe the increase in mass of the electrode for the stages b1−b2 to the accumulation (trapping) of the negatively charged carriers which gives rise to the simultaneous presence of accumulated (trapped) cations necessary for the preservation of the electrical neutrality of the polymer. Since the experimentally measured change in the film's mass exceeds that calculated for the insertion of nonsolvated cations (according to the Faraday law), the excess of the mass is ascribed to accumulation of the solvent molecules. The trapped charge, calculated from the difference between the cathodic and the reverse anodic charges obtained by integration of each CV curve in stages b1−b2 and b3−b4, is listed in Table 2. From this table and Figure 1A it can be concluded that the electronic charge carriers, the compensating counterions (cations), and the solvent molecules, accumulated in the film in stages b1−b2,

**TABLE 2: Amount of Trapped and Detrapped Charges and Masses of the Cation and Solvent Attained**

| cycle group no. | $Q_{trap}$/mC cm$^{-2}$ | $m_{TEA}{}^+$/nmol cm$^{-2}$ | $m_{solv}$/nmol cm$^{-2}$ |
|---|---|---|---|
| b1 + b2 | 0.25 | 2.6 | 26.3 |
| b3 + b4 | 1.0 | 10.4 | 15.2 |
| c1 + c2[a] | −1.0 | −10.4 | −17.1 |

[a] Stage c1 and c2 relates to detrapping of the $TEA^+$ cations and the solvent molecules accumulated during the preceding consecutive n-doping stages (b1−b4). For this reason, the charge density and the mass changes for the cations and solvent in columns 2−4 have negative sign.

result in a well-developed, swelled state of the film: the subsequent cycles show a gradual mass increase along with practically unchanged shape of the CVs and leveling off the FE of the doping-undoping process, see Figure 1A and Tables 1 and 2. On the basis of the experimental mass vs time plots shown in Figure 1A and the Faraday law, the accumulation of the cations and solvent in the film in stages b1−b2 and b3−b4 was presented in molar quantities (i.e., in nmol cm$^{-2}$, see Table 2). It is seen that the preconditioning of the effective n-doping of the film in stages b1 + b2 is a rather small trapping of cations accompanied by its extensive swelling.

In the subsequent n-doping test, b3−b4, the cathodic vertex potential was lowered by 30 mV so that the CV response readily stabilized as cycling proceeded (see the curves b3−6 and b4−6 in Figure 2), showing the FE of 83%. The trapped charge in these steps of the higher cathodic polarization appeared to be considerably larger than in the previous stages b1−b2, amounting to 1 mC cm$^{-2}$, which corresponds to 10.4 nmol cm$^{-2}$ of $TEA^+$ cations and 15.2 nmol cm$^{-2}$ of the accumulated solvent (Table 2). The cations and solvent molecules entrapped in the film were probed in the reverse process of p-redoping (between 1.8 and 4.13 V, stages c1 and c2, see the related CVs in the right corner of Figure 2). It is seen that the n-type trapped charges (1 mC cm$^{-2}$) are quantitatively released during the first charging scan to 4.13 V by outfluxes of the same amount of the accumulated $TEA^+$ and almost the same amount of solvent (Table 2).

The CVs for the freshly p-doped film (a1−3) are very close to that obtained at the end of the c2 test (c2−6, Figure 2), the mass changes are also similar; however, two important features should be noted: (i) the mass change response started to be slower in stage c2 compared to that in stage a1 and (ii) the p-doping in stage c2 (as compared to a1) occurs in the presence of excessive solvent content accumulated in the film's bulk. Trying to get more information on the charge and mass changes during the cycling test, the film was probed under the coupled n-p-doping conditions (i.e., in two-cycle stages d1 and d2). The difference between these stages and the separate stages a, b, and c is that the intermittent condition of cycling may provide insufficient time (depending on the scan rate) for initiating and further advancing the n-doping process, since, as we saw with the stages b1−b2, the kinetics of this process is much slower than that of the p-doping. As seen from Figure 1B, there are periodic mass changes with time (potential), which are interpreted later, in terms of the counterions, co-ions, and solvent fluxes. The CVs for the coupled n-p-doping together with the CV of the separately p- and n-doped film are shown in Figure 3. After the first scan to the cathodic vertex potential (d2−1) there is release of the trapped n-type carriers during the p-redoping close to the potential 3.8 V. However, starting from the second cycle, a stationary response is established with a nucleation loop on the CV for the n-doped film; there is also

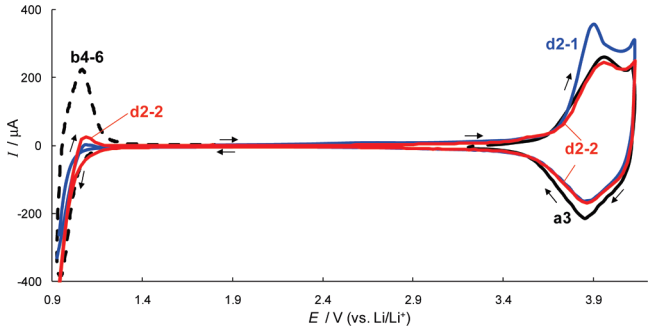


**Figure 3.** A series of CVs for the P3OTh film measured simultaneously with the EQCM response for the coupled n-p-doping stage of the entire test in the potential range between −0.93 and 4.13 V at $\nu = 100$ mV $s^{-1}$ (the first and the second cycles are shown by the blue and the red curves, respectively; the third and subsequent cycles coincided with the second cycle (for clarity not shown in the figure)). p- and n-doping of the fresh film in their native potential domains are shown by the black solid and broken lines, respectively.

virtual coincidence of the anodic part of the CV for the p-redoped film with that of the fresh film, and by 10 −15% lesser charge for the cathodic (undoping) part of the same curve (compare the red and black curves d2−2 and a3−1, respectively, in Figure 3). Certainly, this kind of behavior should stem from the features of the ionic transport during the coupled n-p-doping of the film.

**Separation of the Ionic and Solvent Fluxes during the Electrodes' Multiple Cycling.** To treat these electrodes' response quantitatively, the last cycle d2−2 is analyzed in detail in Figure 4. Following the differential analysis of the mass changes contributing to the doping processes in perm-selective ECP films proposed in ref 30, we present the time derivative of the total mass change, which defines the total flux, $m'(T)$, as sum of that due to ions (calculated from the CV response), $m'(I) = i/zF$), and the solvent, $m'(S)$

$$m'(T) = m'(I) + m'(S) \tag{1}$$

where $i$ denotes CV current and $z$ and $F$ are the ion's charge and the Faraday number, respectively.

The ionic fluxes in moles per second are recalculated taking into account the related molecular weights of both species. It is convenient to normalize the total flux with respect to the molecular weight of the ion[30]

$$J_T = m'_T/M_A \tag{2}$$

$$J_I = m'_I/M_I = i/zF \tag{3}$$

$$J_S = m'_S/M_S = (M_I/M_S)(J_T - J_I) \tag{4}$$

Figure 4A shows the ionic flux calculated using eq 3. Four different colors of the portions of the curve mark the participation of principal counterions and co-ions in the charge compensation mechanism, deconvoluted on the basis of the analysis of the potential dependences of the total charge, $Q$ (panel B), and the character of the mass changes, $m$ (panel C). The dotted black lines in panel B show the charge vs potential plots for the p- and n-doped film in their native potential domains, for the comparison. By starting the cathodic potential scan from 1.2 V toward the vertex potential to 0.9 V and reversing in the anodic direction up to 1.054 V, we note that the CV is expressed

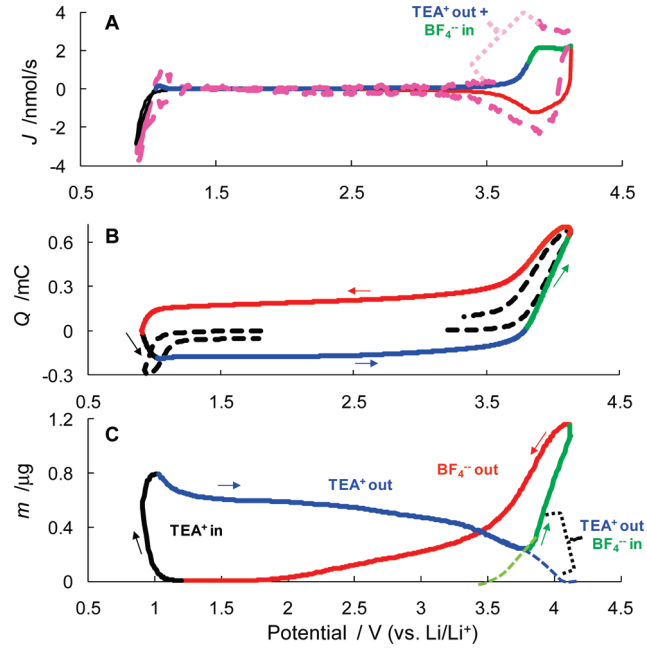


**Figure 4.** Quantitative treatment of the CV and EQCM responses for the coupled n-p-doping stage of the film's cycling life (the curves d2−2 in Figures 3 and 1A, respectively). The panels A, B, and C show the plots of the ionic (and solvent) fluxes, redox-charge of the film, and its mass changes vs potential, respectively. Four different colors are used to identify the nature and direction of the counterions and co-ions fluxes as indicated. In panel A the ionic fluxes (nmol $s^{-1}$) were calculated from the related CV using eq 3. The solvent flux was calculated using equation (4). The region of the cation−anion mixing near 3.8 V during the positive potential scan for which the individual ionic fluxes cannot be precisely separated, and hence, the solvent flux cannot be determined, is indicated by the dotted bracket. For the n-doping the direction of the ionic and solvent flux were reverted in accordance with sign of the current (e.g., during the forward cathodic potential scan the current is negative, which is accompanied by the positive ionic and solvent fluxes; they are, however, shown as negative as the current itself).

by a nucleation-type loop with the cathodic charge and mass increase (shown by the black color of the related curves), attributed to the insertion of $TEA^+$ cations during the n-doping (vide infra). Further anodic potential scan to 3.8 V (the blue portion of the curve) relates to deinsertion of $TEA^+$ cations from the polymer bulk. The scan up to the vertex potential of 4.13 V (the green portion of the curve) relates to the anions insertion into the film, as can be suspected from the change of the sign of the derivative of the mass with respect to potential (panel C). The following cathodic potential scan down to 1.2 V (the red portion of the curve) is due to deinsertion of anions. Since both the charge and mass vs potential plots present complete loops, the mass of the inserted ions should be equal to that for the deinserted ions during undoping process. This makes clear that the border between the blue and the green portions of the curve in panel C (i.e., the vicinity of the minimum) should be assigned to a mixed cation deinsertion and anion insertion, as shown tentatively by the broken blue and the green lines, respectively. As is seen from Figure 4B, the charge due to deinserted cations is equal to the charge for the cations insertion taken from the vertex potential of 0.9 V; however, at higher potentials of the p-doping region, a part of the charge is due to the continued deinsertion of (the deeper trapped) cations, and the rest is due to the insertion of anions. This explains both the shapes of the CVs in panel A (when compared the CV of the freshly p-doped film), and the existence of the cation−anion mixing near the potential of 3.8 V.

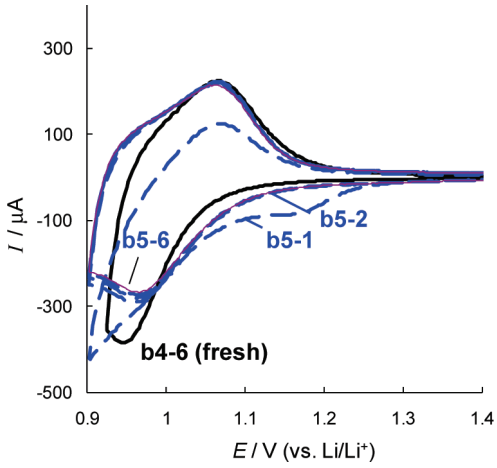


**Figure 5.** The final stage of the cycling test showing 6 consecutive CVs measured at 100 mV $s^{-1}$ (the blue curves as indicated). The black curve shows n-doping behavior of the fresh film for comparison.

The above assignment of the ionic fluxes is further confirmed by determination of the solvent flux for the entire potential range except for the range of the mixed ions transport (when calculated ionic fluxes in nmol $s^{-1}$, the molecular weights of the cation and anions were used for the differently colored portions of the curve in Figure 4A, as indicated above). The calculated solvent flux is shown by the broken rose curve in Figure 4A. It is seen that this flux exceeds somewhat that of the ions at most potentials and hence can serve as a probe of the cycling efficiency of the film. Note also that in this study of the coupled n-p-doping of the P3OTh film we use ionic dynamics (as reflected by EQCM) together with the electroneutrality condition as a diagnostic means to probe the destination of the injected electronic charge (both reversible and trapped, in our case). This exceptionally important feature of the EQCM analysis has been already clearly demonstrated with poly(bithiophene)/poly(xylylviologen) (PBT/PXV) bilayer electrodes,[33] which are much more complicated than the coupled n-p-doping of the single-layer P3OTh film electrodes studied herein; however, one can note a broad similarity in the shape of the CV curves and in the charge and mass versus potential curves for both systems.

The final stage of the cycling test of the P3OTh film electrodes consisted of repeated n-doping cycles (stage b5) after the coupled n-p-doping. As shown in Figure 5, although some changes in the shape of the cathodic portion of the CV curve was observed (compared to that for the fresh film), the doping level decreased only negligibly. In contrast, as seen from Figure 1B, the amplitude of the periodic mass changes in stage b5 is considerably less than that in stages b3−b4 (Figure 1A). The ions and solvent fluxes calculated with the use of eqs 3 and 4, respectively, for the different stages of the cycling life of the film are shown in Figure 6. It is seen that the ionic fluxes for both p- and n-doping of the fresh film are accompanied by (in average) 3−4 times higher flux of the solvent molecules in the same direction (i.e., by influxes and outfluxes during the doping and undoping processes, respectively). As follows from parts B and C of Figure 5, after p-redoping, the flux of solvent molecules decreases (in comparison to that of the fresh film) within the native potential domain of the p-doping and almost completely disappears under the repeated n-doping.

**Changes in the Electronic Structure of the Polymer Film Induced by Long-Term Cycling under Different Conditions.** An important question arises whether or not the variations in the exchangeable solvent content in the film (during a separate cycle) or in the accumulated amount of solvent in the film's bulk at different stages of the film's cycling life correlate with possible changes in the chemical structure and electronic properties of the P3OTh films. Following this purpose, the negative charges trapped in the film during the stages b1−b4 were probed by impedance spectroscopy just before and immediately after the p-redoping test (c1−c2). This was carried out in a separate experiment with a Pt wire covered with a P3OTh film of a similar thickness (as that of the aforementioned electrodes).

As shown in insert b of Figure 2, accumulation of the trapped charges together with solvent in stages b1−b4 results in a drastic increase of the film's impedance (see the blue curve c1−1 measured prior to p-redoping). After the p-redoping, the impedance is only negligibly higher than that for the fresh film measured at the same potential (c1−2 and a1−3, respectively). UV−vis absorption spectroscopy is a sensitive tool of probing the electronic structure of conducting polymers.[34] A P3OTh film deposited onto ITO electrode was studied in the fresh state and after p-redoping of the preliminary n-doped film (insert c in Figure 2). The absorption maximum shifts toward lower wavelengths after the n-doping and the subsequent p-redoping. This can be generally explained by the fact that despite the p-redoping and complete removal of the n-trapped charges the polymer structure has a "conformational memory" of the previous stage of the deeply trapped n-type carriers (vide infra). The spectroscopic data can be interpreted in terms of the polymer possessing effectively a lower conjugation length compared to that of the fresh film. In this situation, in situ conductivity characterization of the film can be very helpful.

In situ conductance technique (for details see our recent paper[35]) was used in order to follow the changes in the films' electronic conductance during its coupled n-p-doping (stages d1−d2), see Figure 7. The n-doped films appear to be about 2 orders of magnitude less conductive than their p-doped counterpart, which is attributed to a localized character of the negative charges on the polymeric backbone rather than to the different doping levels (the latter are of the same order of magnitude). Simultaneous CV and electronic conductivity experiments, with typical results shown in Figure 7, were performed strictly under the same conditions as that for the EQCM coupled with CV experiments (Figure 3). The electronic conductance further drastically decreases as the consecutive n-doping in its native potential domain is changed by the coupled n-p-doping (the blue and the red curves in Figure 7). This shows that a sufficiently effective n-doping process between 1.2 and 0.9 V (as follows from the stages b2−b4 of the EQCM experiments) is possible only with the "mature" well-swelled film with a rather high electronic conductivity. When coming to this domain from the p-doped state of the film, this mature swelled film is not formed at the time scale of the CV scan applied, leaving the n-doping level and hence the electronic conductivity at a low level. We have confirmed the fact of slow formation of the n-doped film by a separate experiment with P3OTh-coated Pt wire (see insert a in Figure 2): when a potential step from 1.8 to 0.82 V was applied, the cathodic current reveals an increase during about 2 s, caused by a nucleation-type process of formation and growth of the swelled n-doped polymer phase of enhanced electronic conductivity. In contrast, upon reversing the potential scan toward positive potentials, only a slight decrease of the conductance is visible during and after the completion of the p-redoping process (the n-trapped charges are removed by this process). This, first, shows that the formation of electronically conductive p-doped zones in the

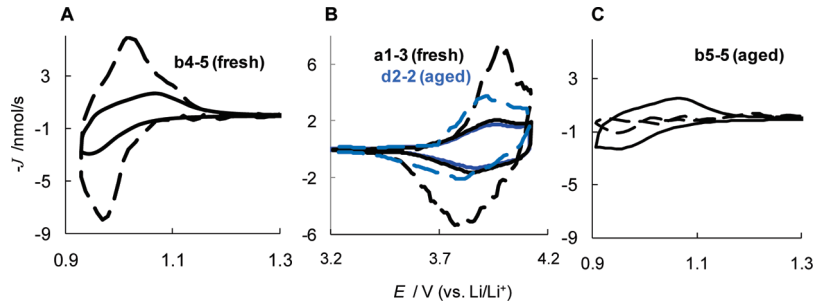


**Figure 6.** The ionic (the solid curves) and the solvent (the broken curves) fluxes calculated from the CV and mass changes of the film electrode using equations (1−4). Panel A relates to the freshly n-doped film; in B the responses of the p-doped fresh and aged film are compared (the black and the blue curves, respectively); C shows the behavior of the n-redoped film at the end of the cycling life.

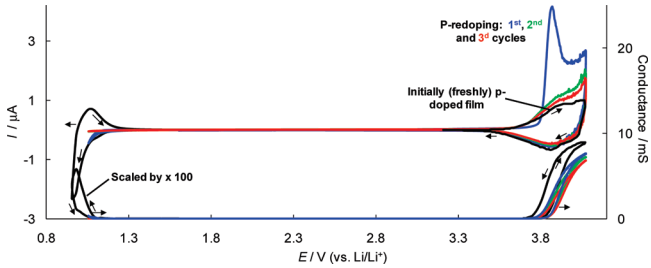


**Figure 7.** Simultaneous CV (the upper curves) and in situ conductance responses (the lower curves) comparing the behavior of the freshly p- and n-doped film's electrodes (the solid black curves) and of the three p-redoping cycles (the blue, green, and red curves, respectively) after the accumulation of negative charge carriers in stages b1−b2 (this test was done similarly to the simultaneous CV and EQCM test shown in Figure 2). Scan rate 100 mV $s^{-1}$.

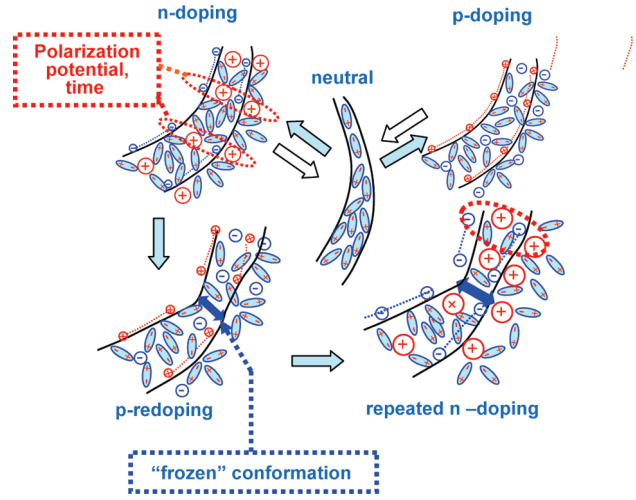


**Figure 8.** Possible molecular scenario of the ionic and solvent transport coupled with conformational changes of P3OTh macromolecules during major stages of the cycling test. Under high and long cathodic polarization the n-type electronic charges are trapped accompanied by the profound changes in the macromolecular conformations (other details are discussed in the text).

film's bulk proceeds at a much faster rate than that with the n-doped counterpart, and, second, the accumulation of the n-trapped charges has a long-term consequence for the p-redoping even after elimination of the trapped charges by high anodic polarization. This result is in a perfect agreement with the impedance and UV−vis characterization of the fresh and the aged films (vide infra). Thus in interpreting the major EQCM feature of the multiple cycled P3OTh films, which is a gradual lost of the exchangeable solvent, we should take into account also the concomitant change in the polymer's electronic structure upon cycling under various cycling conditions.

**Features of the Multiple Doping Mechanism.** Figure 8 suggests a schematic mechanism of changes in the cycling ability of the P3OTh film electrodes under various conditions. Oxidation of the neutral polymer (p-doping, stage a1) is completely reversible with the influx of anions and solvent molecules shown in Figure 6 (the curve a1−3). Well developed, swelled P3OTh films (stages b3−b4) also demonstrate a quasi-reversible n-doping behavior; however, in contrast to the p-doping, as the cathodic polarization and/or polarization time increases, a progressive number of negatively charged carriers are trapped and do not release when cycling in the native potential domain of the n-doped polymer. Formation of the trapped n-type electronic charge carriers should be accompanied by a creation of the favorable local conformation of the macromolecules due to a strong electrostatic attraction between the carrier and the neighboring cation which stiffens the film.[22] Our basic assumption shown schematically in Figure 8 is that after the trapped n-type carriers are completely released during the p-redoping (stages c1−c2) the local macromolecular conformation created during trapping of the n-type carriers remains unchanged (frozen).

In verification of this assumption, we use the generally accepted sequence of 4 separate stages (based on their typical characteristic time constants) constituting the doping processes in ECPs:[22] (i) The electron and ion transfers across the current collector/film and solution/film interfaces; (ii) the coupled electronic and ionic transport from the interfaces to the film's interior as the doping process advances; (iii) the solvent transfer in order to keep activity and/or volume constraints of the film;[22] and (iv) the conformational rearrangement of the macromolecules to satisfy the changes in the electronic charge, and neighboring ionic and solvent surroundings.[22,36] However, this view should be combined with the view of the origin of the n-trapped carriers in conducting polymers. On the basis of a careful analysis of quantum-mechanical and experimental data with various n-doped polythiophene-based polymers, it was concluded that trapping of the n-type carriers originates from very weak intermolecular $\pi$-interaction as contrasts to the very strong intermolecular $\pi$-interactions of their p-doped counterparts.[37] We have furnished experimental evidence that the n-type carriers trapping aggravates considerably under the high cathodic polarization and during a long polarization time. This time is generally required to form a stable complex consisting of the trapped electronic carrier on the macromolecular chain, the compensating counterion (cation), the surrounding solvent molecules, and finally, the appropriate conformation of the macromolecule. The formation of such complexes, locally stiffening the film, can be traced by a gradual decrease of the n-type electronic conductance under continuous cycling, which was especially pronounced with a donor−acceptor type of the

copolymer consisted of alternating octylthiophene and oxadiazole units.[35,38] This copolymer demonstrated exceptionally good stability at high cathodic polarizations with high electronic conductance at the beginning of the n-doping, which eventually decreases under continuous cycling without even a minor decrease in its doping level. Previous experiments with poly(3-fluorophenyl)thiophene revealed that the macromolecular conformations, favoring the electronic carriers trapping are strongly dependent on the solvent nature: the most pronounced effect was caused by acetonitrile, the least was observed with sulfolane.[39,40]

In the present work, we presented evidence of the accumulation of the trapped n-type charge carriers in P3OTh films and their subsequent complete release, using EQCM in its direct gravimetric mode. Moreover, because of the high sensitivity of this technique, we were able to interpret quantitatively the EQCM response in the coupled n-p-doping modes of the P3OTh films. Although the amount of the trapped negative charges during the n-p-doping mode is much less than that during the consecutive n-doping in its native potential domain, we were able to detect the release of the trapped cations at high positive potentials in parallel to the insertion of the anions.

We have established that the progressive loss of the exchangeable solvent content in the film during its cycling life correlates well with the considerable decreases of its electronic conductance, especially during the consecutive n-doping under the high cathodic polarization. In contrast to the case of a conventional redox-polymer, poly(vinylferrocene), in which trapping of the bulky ions occurs owing to the accessible free volume constrain,[41] the n-type carriers trapping in conducting polymers occurs via formation of their very stable complexes with the counterions, solvent molecules and macromolecular conformations as outlined above. The characteristic time of the macromolecular conformational changes is the largest among that for the other contributing processes, so that after removal of the trapped charges, the conformation, typical for the trapped cations, still remains (i.e., is frozen), see Figure 8. This effectively decreases the amount of the exchangeable solvent molecules (accompanying the doping process) and can be regarded as a typical feature of the aged film. The final stage of the film's aging is a loss of its flexibility because of the lack of "plasticizing" solvent molecules, which, in turn, accelerates the cations trapping and further deteriorates the film's cycling performance. Despite the fact that some specially designed donor−acceptor type copolymers may appear to be exceptionally stable to over-reduction (the features of the related ion/solvent transport are unknown), we believe that even in this case, it is unlikely to completely suppress trapping of the n-type charge carriers. For this reason, attention should be paid to the p-dopable ECPs, which can, in principle, compete with inorganic insertion electrodes for practical applications in advanced EDLC cells.

**New Prospects for Improvements of Cycling Efficiency of p-Dopable $\pi$-Conjugated Polymers.** We have herein demonstrated that stable, reproducible cycling of the fresh p-doped P3OTh films requires 3−4 mols of solvent per mol of inserted anions. This ratio rather reflects the selected cycling conditions of the film under consideration, characterized by certain morphology and chemical and electronic structure; this does not mean that the film obtained under different conditions would have the same ratio of the solvent to ion flux. This is because the solvent flux during the doping of the ECPs films, depending on the activity and the volume constrains, is not directly linked to the ionic fluxes.[20,22] This circumstance paves the way for a radical improvement of the cyclability of the p-doped $\pi$-conjugated conducting polymer electrodes. In the case of inorganic Li-ion insertion electrodes, it is well-known that the potential induced dimensional changes are harmful for the electrodes cycling efficiency and life, e.g., microcrystalline Si anode has very high theoretical capacitance (4200 mAh $g^{-1}$); however, it suffers from strong volume expansion (400%), and poor cyclability.[42] In contrast, microcrystalline lithiated titanate spinel, $Li_4Ti_5O_{12}$, with almost zero volume changes during Li-insertion/deinsertion, has excellent cyclability.[43] It was recently demonstrated that Si cathode may dramatically improve its cyclability when grown directly on a current collector in the form of nanowired coating.[44] This is believed to be a general rule to circumvent the capacity failure when large volume changes are involved in intercalation processes into inorganic host materials.

It seems that similar methods can be used to improve cyclability of the ECP cathodes. It should be noted, however, that organic polymers in contact with the inorganic intercalation hosts present soft rather than solid matters, which only increases the number of possible means leading to the desired, improved cyclability compared to the inorganic insertion hosts. Note that small volume changes, required for a polymer cathode to exhibit good cyclability, is just the opposite requirement for building an effective gas sensor or actuator on the basis of conducting polymers.[45] Fortunately, the powerful arsenal of the modern organic chemistry, electrochemistry and material sciences allows meeting different, even conflicting demands. The range of possible means, which may improve the ECPs cyclability, widely varies from the earlier attempts to prepare beneficial composite electrodes with conventional polymers, such as carbomethylcellulose,[46] polymeric ionomers, such as Nafion,[26] cross-linked polymeric gels (elastomers),[47] template synthesis of the ECP nanostructures using the "track-etch" membranes[48] up to the recent template syntheses with the use of mesoporous carbon monolith[49] and carbon foam.[50] In all these cases, for rare exceptions, the cyclability tests have not been carried out. However, recently, the improved cyclability of the ECPs has been discovered, when they are used as nanocomposites. This includes nanocomposites of conducting polymers with amorphous $MnO_x$,[51] $TiO_2$,[52] and self-assembled colloidal templates.[53] The fullerene-doped ECPs[54] and the carbon nanotubes covalently or noncovalently attached to the ECPs[55,56] seem to be very attractive in view of their enhanced cyclability. Whether stabilization of cycling behavior of the ECPs in such nanocomposites is linked to the diminished solvent transport is a real challenge for future advanced applications of EQCM.

## Conclusion

We report herein new results on application of the EQCM method to study multiple p- and n-doping of the P3OTh film electrodes under various cycling conditions. Emphasis is given to the n-doping process with its initial slow kinetics caused by the accumulation of cations and solvent molecules to produce well-developed, swelled films. The trapped cations and part of the solvent content were shown to be quantitatively released only at high anodic polarizations. The conditions were then moderated by performing a coupled (intermittent) n-p-doping with the complete deconvolution of the EQCM response in terms of counterions, co-ion, and solvent fluxes. A remarkable feature that we observed was a gradual decrease of the exchangeable solvent content in the film's bulk as a result of the film's multiple cycling. To correlate the failure of the aged films to accommodate as much solvent as was in their fresh state with possible

changes in the film's chemical and electronic structure, the electrochemical impedance, in situ UV−vis spectroscopy, and in situ electronic conductance measurements were employed. On the basis of the results obtained, frozen conformations of the macromolecules arising during multiple n-doping of the film and remaining even after removal of trapped cations were suspected to be the origin of the free volume constrains within the polymeric fibrils. This diminishes the amount of the exchangeable solvent molecules during subsequent cycling the films without a considerable change in the films' doping level, which is an early indication of the commencing process of their aging. We tried to apply the obtained information on the ions and solvent molecules fluxes, accompanying the doping processes in the conducting polymers, for the comparison between the cycling efficiency of the ECP film electrodes and the efficiency of typical ion-insertion electrodes used in rechargeable batteries and asymmetric EDLC cells. A next development that can be very useful is a fabrication of nanocomposite active mass, comprising carbon nanotubes and ECP. Derivatized poly thiophene films are very good candidates for these electro-active composites. On the basis of the studies presented herein, it is clear that EQCM can serve as a very useful technique for investigating the cycling behavior of such nanocomposite electrodes.

## Experimental Section

**Covering Pt-Coated AT-Cut 5-MHz Maxtek's 1-in. Diameter Quartz Crystal with Thin P3OTh Films.** The polymer films suitable for gravimetric EQCM applications were prepared by anodic galvanostatic polymerization in a three-electrode electrochemical cell. 3-Octylthiophene (Aldrich, analytical grade used without further purification) in a concentration of 0.1 M was dissolved in 2:8 volume ratio of $CH_2Cl_2$ and propylene carbonate mixture containing 0.1 M $TEABF_4$. Surface area of the plated crystal for the film's deposition was 1.37 $cm^2$; the current applied for the polymerization was 0.426 mA for the periods of time of 30, 60, or 100 s. Two thinner films showed purely gravimetric response, including the multiple n-doping, whereas for the thickest film an increase of the crystal resistance at the end of the n-doping was observed. On the basis of the estimation of the coated film's mass by EQCM, the thinnest film weighs 5.5 $\mu g\ cm^{-2}$ (28.4 nmol $cm^{-2}$). By assumption of the P3OTh film's density as 1 g $cm^{-3}$, the thickness was estimated as 50 nm. The values of the redox charges and the mass changes for all 3 films were proportional to the deposition time. The estimated value of the p-doping level (the charge per repeat unit of the polymer) was close to 0.24. The present paper reports the data related to a P3OTh film 100 nm thick (60 s deposition time).

**Instrumentation and Methods.** Potential scanning and current recording during CV, EQCM, and EIS measurements were carried out with the use of a computerized potentiostat-galvanostat Model 20 Autolab with a FRA module (controlled by the GPES Version 4.8 Eco Chemie B.V. Software (Utrecht, The Netherlands)). Impedance spectra were measured from 500 kHz to 10 mHz, with a 5-mV peak-to-peak alternative voltage after a full equilibration of the cell. Frequency changes during the film's doping were registered using Maxtek RQCM system, allowing also simultaneous monitoring of the crystal resistance (a significant increase of this resistance signifies the transition from acoustically thin to acoustically thick film behavior).The Sauerbrey equation was applied to convert the frequency shift into mass changes: $\Delta f = -C_f \Delta m$, where $C_f$ is the sensitivity factor of the crystal ($C_f = 0.056$ Hz/ng/$cm^2$) and $\Delta m$ is the change in mass of the coating per $cm^2$.

In situ conductance measurements were performed with the use of an interdigitated Pt microarray electrode (Abtech Scientific (VA)). Each microelectrode in the array was 5 $\mu$m wide and 3 mm long, separated by 5 $\mu$m insulating gaps between the adjacent bands. These gaps were bridged by the film during electropolymerization process in the monomer-containing solution of the same composition as that for the film's deposition onto a quart crystal. Details of the calculation of conductance and the CV current, using measurements with bipotentiostat module, and the in situ optical absorption studies with the use of a P3OTh coated ITO have been recently reported.[35]

**Acknowledgment.** M.L. acknowledges the Royal Society of Chemistry for awarding him with a Journals Grant for International Authors (Application No. 08-01-603).

## References and Notes

(1) *Handbook of Conducting Polymers. Conjugated Polymers. Theory, Synthesis, Properties and Characterization*, 3rd ed.; Skotheim, T. A., Reynolds, J. R., Eds.: CRC Press: Boca Raton, FL, 2007.
(2) Inzelt, G. *Conducting Polymers. A New Era in Electrochemistry*; Scholz, F., Ed.: Springer-Verlag: 2008.
(3) Heinze, J. *Top. Curr. Chem.* **1990**, *2*, 1–47.
(4) (a) Roncali, J. *Chem. Rev.* **1992**, *92*, 711–738. (b) Roncali, J. *Chem. Rev.* **1997**, *97*, 173–205.
(5) Leclerc, M. *30 Years of Conducting Polymers*. *Macromol. Rapid Commun.* **2007**, *28*, 1665–1824.
(6) *Conductive Polymers and Plastics in Industrial Applications*, Rupprecht, L., Ed.: Plastics Design Library, 1999.
(7) *Conductive Electroactive Polymers: Intelligent Materials Systems*, 2nd ed. Wallace, G. G., Spinks, G. M., Kane-Maquire, L. A. P., Teasdale, P. R., Eds.: CRS Press, NY, 2003.
(8) Shirakawa, H.; Louis, E. J.; Mac-Diarmid, A. G.; Chiang, C. K.; Heeger, A. J. *Chem. Commun.* **1977**, 578–580.
(9) *Conjugated Polymer and Molecular Interfaces*, Salaneck, W. R., Seki, K., Kahn, A., Pireaux, J., Eds.: Marcel Decker, 2002.
(10) Lee, K.; Cho, S. H.; Heeger, A. J.; Lee, C. W.; Lee, S. H. *Nature* **2006**, *441*, 65–68.
(11) Sheats, J. R. *J. Mater. Res.* **2004**, *19*, 1974–1994.
(12) Pron, A.; Rannou, P. *Prog. Polym. Sci.* **2004**, *27*, 135–190.
(13) Tadanori, K.; Chu-Chen, C.; Cheng-Liang, L.; Tomoya, H.; Mitsuru, U.; Wen-Chang, C. *Macromolecules* **2010**, *43*, 1236–1244.
(14) Yen-Ju, C.; Sheng-Hsiung, Y.; Chain-Shu, H. *Chem. Rev.* **2009**, *109*, 5868–5923.
(15) Pron, A.; Gawrys, P.; Zagorska, M.; Djurado, D.; Demadrille, R. *Chem. Soc. Rev.* **2010**, *39*, 2577–2632.
(16) Horowitz, G. *J. Mater. Res.* **2004**, *19*, 1946–1962.
(17) See for a review: *Adv. Mater.*, 2009, *21*, issues 14−15.
(18) Osaka, I.; McCullough, R. D. *Acc. Chem. Res.* **2008**, *41*, 1202–1214.
(19) Sirringhaus, H.; Tessler, N.; Friend, R. H. *Science* **1998**, *280*, 1741–1744.
(20) Bruckenstein, S.; Hillman, A. R. *J. Phys. Chem.* **1988**, *92*, 4837–4839.
(21) Hillman, A. R.; Mohamoud, M. A.; Bruckenstein, S. *Electroanalysis* **2005**, *17*, 1421–1432.
(22) Hillman, A. R.; Efimov, I.; Skompska, M. *Faraday Discuss.* **2002**, *121*, 423–439.
(23) Suarez, M. F.; Compton, R. G. *J. Electroanal. Chem.* **1999**, *462*, 211–221.
(24) Mansunaga, T.; Daifuku, H.; Nakajima, T.; Kawagoe, T. *Polym. Adv. Technol.* **1989**, *1*, 33–39.
(25) Yue, J.; Epstein, A. J. *J. Am. Chem. Soc.* **1990**, *112*, 2800–2801.
(26) Nagasubramanian, G.; Di Stefano, S.; Moacanin, J. *J. Phys. Chem.* **1986**, *90*, 4447–4451.
(27) Novak, P.; Muller, K.; Santhanam, K. S. V.; Haas, O. *Chem. Rev.* **1997**, *97*, 207–281.
(28) Kang, B.; Ceder, G. *Nature* **2009**, *458*, 190–193.
(29) *Carbon for Electrochemical Energy Storage and Conversion Systems*, Beguin, F., Frackowiak, E., Eds.; CRS Press: NY, 2010.
(30) Hillman, A. R.; Daisley, S. J.; Bruckenstein, S. *Electrochim. Acta* **2008**, *53*, 3763–3771.
(31) Akieh, M. N.; Price, W. E.; Bobacka, J.; Ivaska, A.; Ralph, S. F. *Synth. Met.* **2009**, *159*, 2590–2598.
(32) Nystrom, G.; Razaq, A.; Stromme, M.; Nyholm, L.; Mihranyan, A. *Nano Lett.* **2009**, *9*, 3635–3639.
(33) Hillman, A. R.; Glidle, A. *Phys. Chem. Chem. Phys.* **2001**, *3*, 3447–3458.

(34) Holze, R. *Surface and Interface Analysis*; Springer: Berlin-Heidelberg, 2009.

(35) Pomeranz, Z.; Levi, M. D.; Salitra, G.; Demadrille, R.; Fisyuk, A.; Zaban, A.; Aurbach, D.; Pron, A. *Phys. Chem. Chem. Phys.* **2008**, *10*, 1032–1042.

(36) Otero, T. F.; Grande, H.; Rodrigues, J. *J. Phys. Chem. B* **1997**, *101*, 8525–8533.

(37) Zotti, G.; Zecchin, S.; Schiavon, G.; Vercelli, B. *Chem. Mater.* **2004**, *16*, 3667–3676.

(38) Levi, M. D.; Fisyuk, A.; Demadrille, R.; Markevich, E.; Gofer, Y.; Aurbach, D.; Pron, A. *Chem. Commun.* **2006**, 3299–3301.

(39) Levi, M. D.; Gofer, Y.; Cherkinsky, M.; Birsa, M. L.; Aurbach, D.; Berlin, A. *Phys. Chem. Chem. Phys.* **2003**, *5*, 2886–2893.

(40) Levi, M. D.; Gofer, Y.; Aurbach, D.; Berlin, A. *Electrochim. Acta* **2004**, *49*, 433–444.

(41) Jureviciute, I.; Bruckenstein, S.; Hillman, A. R. *J. Electroanal. Chem.* **2000**, *488*, 73–81.

(42) Vincent, C. A.; Scrosati, B. *Modern Batteries. An Introduction to Electrochemical Power Sources*, 2nd ed., Butterworth-Heinemann: Oxford, 1997.

(43) Yi, T. F.; Shu, J.; Zhu, Y. R.; Zhu, X. D.; Zhu, R. S.; Zhou, A. N. *J. Power Sources* **2010**, *195*, 285–288.

(44) Chan, C. K.; Peng, H.; Liu, G.; McIlwrath, K.; Zhang, X. F.; Huggins, R. A.; Cui, Y. *Nature Nanotechnol.* **2008**, *3*, 31–35.

(45) Jager, E. W. H.; Smela, E.; Inganas, O. *Science* **2000**, *290*, 1540–1545.

(46) Otero, T. F.; Herrasti, P.; Ocon, P.; Alves, C. R. *Electrochim. Acta* **1998**, *43*, 1089–1100.

(47) Shankar, R.; Ghosh, T. K.; Spontak, R. J. *Soft Matter* **2007**, *3*, 1116–1129.

(48) Martin, C. R. *Acc. Chem. Res.* **1995**, *28*, 61–68.

(49) Fan, L.-Z.; Hu, Y.-S.; Maier, J.; Adelhelm, P.; Smarsly, B.; Antonietti, M. *Adv. Funct. Mat.* **2008**, *17*, 3083–3087.

(50) Zhang, Q. W.; Zhou, X.; Yang, H. S. *J. Power Sources* **2004**, *125*, 141–147.

(51) Sun, L.-J.; Liu, X.-X.; Lau, K. K. T.; Chen, L.; Gu, W.-M. *Electrochim. Acta* **2008**, *53*, 3036–3042.

(52) Xu, H.; Cao, Q.; Wang, X.; Li, W.; Li, X.; Deng, H. *Mater. Sci. Eng., B* **2100**, *171*, 104–108.

(53) Bartlett, P. N.; Birkin, P. R.; Ghanem, M. A.; Toh, C.-S. *J. Mater. Chem.* **2001**, *11*, 849–853.

(54) Wang, C.; Guo, Z.-X.; Fu, S.; Wu, W.; Zhu, D. *Prog. Polym. Sci.* **2004**, *29*, 1079–1141.

(55) Frackowiak, E.; Khomenko, V.; Jurewicz, K.; Lota, K.; Beguin, F. *J. Power Sources* **2006**, *153*, 413–418.

(56) Baibarac, M.; Gomez-Romero, P.; Lira-Cantu, M.; Casan-Pastor, N.; Mestres, N.; Lefrant, S. *Eur. Polym. J.* **2006**, *42*, 2302–2312.

JP105965U